Density-functional theory of a lattice-gas model with vapour, liquid, and solid phases

2003 J. Phys.: Condens. Matter 15 3931

(http://iopscience.iop.org/0953-8984/15/23/308)

INSTITUTE OF PHYSICS PUBLISHING JOURNAL OF PHYSICS: CONDENSED MATTER

J. Phys.: Condens. Matter **15** (2003) 3931–3956 PII: S0953-8984(03)62621-4

Density-functional theory of a lattice-gas model with vapour, liquid, and solid phases

Santi Prestipino[1] **and Paolo V Giaquinta**

Istituto Nazionale per la Fisica della Materia (INFM), Unità di Ricerca di Messina, Italy
and
Università degli Studi di Messina, Dipartimento di Fisica, Contrada Papardo,
98166 Messina, Italy

E-mail: Santi.Prestipino@unime.it

Received 24 April 2003
Published 30 May 2003
Online at stacks.iop.org/JPhysCM/15/3931

Abstract

We use the classical version of the density-functional theory in the weighted-density approximation to build up the entire phase diagram and the interface structure of a two-dimensional lattice-gas model which is known, from previous studies, to possess three stable phases—solid, liquid, and vapour. Following the common practice, the attractive part of the potential is treated in a mean-field-like fashion, although with different prescriptions for the solid and the fluid phases. It turns out that the present theory, compared to similar theories in the continuum, is of worse quality. Nevertheless, at least a number of qualitative facts are reproduced correctly: (i) the existence of three phases; (ii) the disappearance of the liquid phase when the range of the attraction is progressively reduced; and (iii) the intrusion, just below the triple-point temperature, of a liquid-like layer at the interface between the coexisting solid and vapour phases.

1. Introduction

Nowadays, most of the theoretical studies of the phase behaviour of a classical fluid are formulated in the language of the density-functional theory (DFT) [1, 2]. Within such a theory, the crystalline solid is viewed as being like an inhomogeneous system with a periodically modulated density profile $n(x)$, whose free energy is obtained through the optimization of a density functional $F[n]$ which is built upon the structural properties of the fluid. In particular, a successful recipe for $F[n]$ (sometimes called the Hohenberg–Kohn–Mermin (HKM) free energy) is a local mapping into the free energy of a homogeneous fluid with a suitably chosen effective density $\bar{n}(x)$, which is related in a non-local way to the real density $n(x)$. At variance with $n(x)$, the smoothed density $\bar{n}(x)$ is a slowly varying function of the position. This general method has been named the 'weighted-density approximation' (WDA) [3, 4].

[1] Author to whom any correspondence should be addressed.

This scheme has proved to be sufficient for purely hard-core systems and soft repulsive ones. However, it fails badly in the presence of attractive interactions, where it may happen that the solid is being mapped onto a fluid with a density falling into the condensation gap where, actually, no homogeneous phase is present. Nor can the fundamental-measure approach of Rosenfeld [5], which was recently extended from hard spheres [5, 6] to spherically repulsive interactions [7] but not yet to attractive fluids, be of help. In these cases, the only available method is lowest-order perturbation theory [1], which is tantamount to splitting the HKM free energy into a sum of the density functional for a reference system (usually, a hard-core system) and a remainder, containing the pair distribution function of the inhomogeneous reference system. A sensible approximation for the latter would allow one to draw accurate coexistence lines for the system under consideration. In the past, a scheme of this sort has been successfully applied by a number of authors to the prototypical case represented by the truncated Lennard-Jones fluid [8–12].

In the present paper, we prove that this method is effective, although with less quantitative success, also for lattice problems. As a case study, we shall focus on a two-dimensional (2D) lattice-gas system which is known [13] to possess three phases with the features of vapour, liquid, and solid. It is argued in [13] that the existence in this model of a further liquid phase, besides the gaseous one, is made possible by the relatively long range of the interparticle attraction. We point out that the choice of a 2D (rather than 3D) system is only aimed at simplifying the forthcoming analysis of the interface problem. In this respect, a crucial test for our DFT will be the prediction of surface melting, which is actually in the range of possibilities of the DFT, as is proved by the 3D continuum theory of [11].

While the general DFT framework on a lattice (i.e., minimum principle for the generalized grand potential plus Ornstein–Zernike (OZ) relation) is already known [14, 15], we are not aware of any single example of the application of the lattice DFT in the WDA for a system with a realistic phase diagram. We believe that testing the degree of sophistication of the lattice-DFT method in a rich context, such as that provided by a three-phase lattice-gas model, can be interesting on fairly general grounds, e.g. for weighing up the superiority, if any, of the DFT over other available statistical methods such as the transfer-matrix [13] and the cluster variational methods [16].

This paper is arranged as follows. After giving an outline, in section 2, of the main contents of the lattice DFT, we describe our system and method in section 3, and present our results for the bulk of the system in section 4. Next, in section 5, we analyse the structure of the interface between two bulk phases, including a demonstration of the phenomenon of surface melting. Further remarks and a brief summary of the main results are given in the conclusions.

2. Lattice density-functional theory

We first review the lattice analogue of the classical DFT, which was first considered by Nieswand *et al* [14]. Like the parent theory in the continuum, the lattice DFT is meant to provide a general framework for discussing the statistical properties of particles existing on a regular lattice, in the presence of a site-dependent external potential or, even, of a self-sustained spatial inhomogeneity (like the one which, in a simple fluid, becomes manifest at freezing). If lattice sites are allowed to be occupied by at most one particle, a general Hamiltonian for our problem is $H + \sum_i \epsilon_i c_i$, with

$$H = \sum_{i<j} v(|i-j|) c_i c_j. \tag{1}$$

We call $c_i = 0, 1$ the occupation number of site i in the lattice, while $v(|i - j|)$ and ϵ_i are the pair interaction and the external potential, respectively.

The grand-canonical partition function

$$\Xi = \sum_{\{c\}} \exp\left(\beta \sum_i (\mu - \epsilon_i) c_i\right) \exp(-\beta H) \tag{2}$$

(with β and μ representing the inverse temperature and the chemical potential, respectively) is a *lattice functional*, namely a function of all components $\mu_i = \mu - \epsilon_i$ of a lattice field, which we call the external field. Then, it is a simple matter to show that the (number-) density field is given by

$$n_i \equiv \langle c_i \rangle = \frac{1}{\Xi} \frac{\partial \Xi}{\partial \beta \mu_i} = -\frac{\partial \Omega}{\partial \mu_i}, \tag{3}$$

which is a functional of the external field (a temperature dependence is also implied). $\Omega = -\beta^{-1} \ln \Xi$ is the grand potential, also a functional of $\{\mu_i\}$. At variance with the continuum case, the density field is a *partial*, rather than a functional, derivative of Ξ.

The HKM theorem, which holds also for lattice gases, ensures that there is a one-to-one correspondence, within the space of μ-representable densities, between the density field and the external field. Thanks to this theorem, the Legendre transform of $\Omega[\mu]$ with respect to its functional variable is a well-defined object, which generalizes the concept of Helmholtz free energy to inhomogeneous situations:

$$F[n] = \Omega[\mu] + \sum_i \mu_i n_i \Big|_{\mu_i = \mu_i[n]}. \tag{4}$$

Another expression for $F[n]$ is obtained by considering

$$\pi[n] = \frac{1}{\Xi} \exp\left(\beta \sum_i \mu_i[n] c_i\right) \exp(-\beta H) \tag{5}$$

(with Ξ evaluated at $\mu_i[n]$), which represents the grand-canonical probability density for the given n, i.e., the one calculated for $\mu_i = \mu_i[n]$. It follows that

$$F[n] = \sum_{\{c\}} \pi[n] \left(H + \frac{1}{\beta} \ln \pi[n]\right). \tag{6}$$

In practice, the ideal-gas system ($H = 0$) is the only lattice system for which the computation of the HKM free energy can be carried out explicitly, with the result

$$\beta F^{id}[n] = \sum_i [n_i \ln n_i + (1 - n_i) \ln(1 - n_i)]. \tag{7}$$

In the general case, $F[n]$ is written as the sum of the ideal term and an excess contribution $F^{exc}[n]$ which is to be approximated in some way.

A further density functional can be defined from $F[n]$, which is a sort of generalized grand potential:

$$\Omega_\mu[\rho] = F[\rho] - \sum_i \mu_i \rho_i = \sum_{\{c\}} \pi[\rho] \left(H + \frac{1}{\beta} \ln \pi[\rho] - \sum_i \mu_i c_i\right), \tag{8}$$

where a different symbol, ρ, is used for the density field to stress the fact that no relation is implied between ρ and μ, which should thus be regarded as independent functional variables. Instead, we reserve the symbol n for the density field derived from μ.

$\Omega_\mu[\rho]$ is actually the inhomogeneous Gibbs–Bogoliubov functional of the classical mean-field theory. Hence, a minimum principle holds, saying that $\Omega_\mu[\rho]$ attains its minimum value

for a density profile which is precisely the one determined by the given external field, namely n. Moreover, the minimum $\Omega_\mu[n]$ is nothing but the grand potential Ω for the given μ. The necessary condition for the minimum reads

$$\left.\frac{\partial \Omega_\mu}{\partial \rho_i}\right|_{\rho_i=n_i} = 0. \tag{9}$$

The minimum principle for $\Omega_\mu[\rho]$ is, besides the HKM theorem, the basic tenet of the DFT, being at the heart of a broad family of approximate theories of freezing [2]. Every such a theory starts from a prescription for $F[n]$, which is then used to determine an approximate grand potential for the system from which the thermodynamic properties are deduced.

We conclude our general presentation of the lattice DFT with the OZ relation. Taking

$$c_i^{(1)}[n] = -\beta \frac{\partial F^{exc}}{\partial n_i} \qquad \text{and} \qquad c_{ij}^{(2)}[n] = \frac{\partial c_i^{(1)}}{\partial n_j} \tag{10}$$

to be the one- and two-point direct correlation function (DCF), respectively, the formal solution of equation (9) reads

$$n_i = \frac{1}{1+\exp\{-\beta\mu_i - c_i^{(1)}[n]\}}. \tag{11}$$

Upon introducing the reduced pair distribution function (PDF),

$$g_{ij} = (1-\delta_{ij})\frac{\langle c_i c_j\rangle}{n_i n_j}, \tag{12}$$

and a further function

$$C_{ij} = c_{ij}^{(2)} - \frac{\delta_{ij}}{1-n_i}, \tag{13}$$

it can be shown [14] that the following relation follows from equation (11):

$$h_{ij} = C_{ij} + \sum_k C_{ik} n_k h_{kj}, \tag{14}$$

which is the lattice OZ relation ($h_{ij} = g_{ij} - 1$ is called the total correlation function). Only a further relation between g and $c^{(2)}$ would allow one to determine both functions. The importance of $c^{(2)}$ is twofold: on one hand, its knowledge permits one to recover, through the OZ relation, the PDF profile. On the other hand, most of the popular DFT approximations use an expression for $F[n]$ in terms of the DCF of the fluid.

A number of simplifications occur for a homogeneous system (i.e., one with $\epsilon = 0$). Owing to translational symmetry, the one-point DCF is a constant, $c_i^{(1)}[n] = c_1(\rho)$, whereas the two-point DCF is a function of $i - j$ only, that is $c_{ij}^{(2)}[n] = c_2(i-j,\rho)$. Furthermore, equation (14) can be Fourier transformed[2] to give $\tilde{h}_q = \sum_x h_x \exp(-\mathrm{i}q\cdot x)$ in terms of $\tilde{C}_q$ as

$$\tilde{h}_q = \frac{\tilde{C}_q}{1-\rho\tilde{C}_q}, \tag{15}$$

ρ being the constant value of the density.

In the next section, we describe a DFT aimed at reconstructing the phase diagram of a realistic lattice gas, that is one with a phase diagram containing, besides a solid phase, also

[2] On a finite $N_x \times N_y$ lattice, the use of periodic boundary conditions makes it possible to expand every field f_x in a (Fourier) series of complex exponentials: $\tilde{f}_q = \sum_x f_x \exp(-\mathrm{i}q\cdot x)$, where the Born–Von Karman vectors $q = q_x b_x + q_y b_y$. The vectors b_x and b_y form a basis of the reciprocal lattice and, e.g., $q_x = m_x/N_x$ with $m_x = -(N_x/2)+1,\ldots,N_x/2$. The inverse relation is $f_x = (1/N)\sum_q \tilde{f}_q \exp(\mathrm{i}q\cdot x)$, $N = N_x N_y$ being the number of lattice sites. A useful property is the convolution theorem $\widetilde{(f*g)}_q = \tilde{f}_q \tilde{g}_q$, where $(f*g)_x = \sum_y f_{x-y} g_y$.

two different fluid phases, liquid, and vapour. In order to condense the discussion, we have decided to confine most of the technicalities to a few appendices. In particular, appendix A illustrates the lattice counterpart of two celebrated, yet simple, theories of freezing: the Ramakrishnan–Yussouff (RY) theory and the Tarazona WDA. We suggest reading appendix A before proceeding to the next section.

3. Model and method

We shall work with the t345 model of [13]. This is a triangular-lattice model with a hard core covering first- and second-neighbour sites and a pair attraction ranging from third- to fifth-neighbour sites (see figure 1 of [13]). The strength of the attraction reduces upon increasing the distance from a reference site: whence, a triangular solid is stable at high density and low temperature, with a maximum density of $\rho_{max} = 0.25$. Upon comparing the solid and the vapour grand potentials, one can easily predict the zero-temperature value of the chemical potential at coexistence to be $\mu_c(T = 0) = 3v_3$, $v_3 < 0$ being the pair-potential value at contact. To be specific, we use hereafter the same v-values as were considered in [13], namely $v_3 = -1.5V$, $v_4 = -1.2V$, and $v_5 = -V$, with $V > 0$. In that paper, a combination of transfer-matrix calculations and Monte Carlo (MC) simulations distinctly showed the existence of a narrow temperature interval where the increase of μ, starting from large negative values, drives the system through a couple of sharp (first-order) phase transitions, i.e., vapour–liquid and liquid–solid, as is also revealed by the μ-evolution of the number-density histogram at fixed temperature. For later convenience, two other models are introduced: the t3 model, which is the same as t345 but with $v_4 = v_5 = 0$, and the t model, where also $v_3 = 0$ and only the hard-core interaction is present. At variance with the t345 case, the MC simulation supports the existence of a unique fluid phase in both the t and t3 models.

The first step in a typical DFT calculation is the determination of an accurate DCF for the homogeneous system. In fact, an approximate $F[n]$ is usually built upon this function (see appendix A). The fluid DCF is the solution to the homogeneous OZ relation plus a closure. For 3D hard spheres, the most celebrated closure of all is the Percus–Yevick approximation (PYA), which allows an exact determination of the DCF [17]. For a lattice system, the mean-spherical approximation (MSA) is easier to implement than the PYA, since it leads to a smaller set of unknown quantities. As a matter of fact, serious convergence problems are encountered when trying to solve numerically either the MSA or the PYA of the t345 fluid. Instead, no such problems occur for the MSA of the t or, even, the t3 model (see the details in appendix B), while the PYA of the t3 model is still intractable. As a result, we are forced to treat the t345 model perturbatively, as we are going to see in a moment (note that our derivation of the perturbation formula, equation (16) below, will be different from that of Evans [1]).

Let us write $v(|i - j|)$ as $v_0(|i - j|) + \Delta v(|i - j|)$, where v_0 describes a reference system, say the t model, and Δv is a remainder. We shall prove that, using a 0 subscript for quantities pertaining to the t model, one has, at the lowest order in β,

$$F[n] = F_0[n] + \sum_{i<j} \Delta v(|i - j|)\, \langle c_i c_j \rangle_0. \tag{16}$$

Let $v_\lambda = v_0 + \lambda\, \Delta v$ be a linear path between v_0 and v, with $0 \leqslant \lambda \leqslant 1$. Accordingly, we define $H_\lambda = H_0 + \lambda\, \Delta H$. Let $\pi_\lambda[n]$ be the grand-canonical probability density of H_λ under the condition that the external field takes precisely that value, $\{\mu_{\lambda i}[n]\}$, which produces a density of n. Next, we define

$$F_\lambda[n] = \sum_{\{c\}} \pi_\lambda[n] \left(H_\lambda + \frac{1}{\beta} \ln \pi_\lambda[n] \right) \tag{17}$$

to be the HKM free energy relative to H_λ.

In the same spirit as classical Zwanzig perturbation theory [17], we derive an approximate expression for $F[n]$ starting from the exact formula

$$F[n] = F_0[n] + \int_0^1 \mathrm{d}\lambda \, \frac{\partial F_\lambda[n]}{\partial \lambda}. \tag{18}$$

A rather lengthy calculation gives

$$\frac{\partial F_\lambda[n]}{\partial \lambda} = \langle \Delta H \rangle_\lambda + \beta[\langle B \rangle_\lambda \langle \Delta H \rangle_\lambda - \langle B \, \Delta H \rangle_\lambda] - \beta[\langle A \rangle_\lambda \langle B \rangle_\lambda - \langle AB \rangle_\lambda], \tag{19}$$

where $\langle \cdots \rangle_\lambda$ is an average over $\pi_\lambda[n]$ and

$$A = \sum_i \frac{\partial \mu_{\lambda i}[n]}{\partial \lambda} c_i \qquad \text{and} \qquad B = \sum_i \mu_{\lambda i}[n] c_i. \tag{20}$$

Considering that $\mu_{\lambda i}[n]$ is unknown, some assumption must be made in order to obtain $F[n]$. In particular, if v_0 is a hard-core interaction, the rhs of equation (19) reduces, at the lowest order in β, to $\langle \Delta H \rangle_0$, yielding eventually equation (16).

We note that, in equation (16), $\langle c_i c_j \rangle_0 = n_i n_j g_{0,ij}[n]$ contains the exact, yet unknown, reduced PDF of the inhomogeneous t model. Hence, the above equation is useless unless one finds a careful prescription for $g_{0,ij}$, which could be possibly *different* for the fluid and solid phases. Before discussing this point further, we go back for a moment to the reference system.

After obtaining the DCF of the homogeneous t system, we use equation (A.3) to calculate the fluid excess free energy per particle $f^{exc}(\rho)$. This quantity, which is a monotonically increasing function of the density, ceases to be defined at $\rho \simeq 0.21$, beyond which no MSA solution is actually found. However, this density is too small for allowing a description (within the WDA) of the very dense solid. Hence, the problem arises as to what criterion should be used in order to extrapolate $f^{exc}(\rho)$ beyond that limit. This problem is discussed in appendix B, where two different solutions are proposed. Here, suffice it to say that there exists a method for producing an extension of the definition of $f^{exc}(\rho)$ insofar as it is needed, with all regularity requirements fully met.

We have sketched in appendix B the details of a simple DFT (the RY theory [18]) for the freezing of the t model. However, in order to obtain a good description of the reference system, we have tried to do better than the RY theory. In fact, the stability of the liquid phase is a matter of a delicate balance between energy and entropy; hence, an accurate representation of the solid free energy is an obvious necessity in all cases where a liquid phase is expected. Leaving aside Rosenfeld's fundamental-measure theory, whose extension to lattice fluids is not immediate (see, however, the recent contribution [19]), we have applied the lattice counterpart of the WDA in the version implemented by Tarazona [3], which gives rather good results for the hard-sphere system. This theory is reviewed in the appendices A (general) and C (t model). Here, we provide just a few details on the method.

The hypothesis underlying any WDA is an approximation of the excess free energy of the system as $\sum_i n_i f^{exc}(\bar{n}_i)$, where the weighted density $\bar{n}_i$ is a non-local functional of the density field, given implicitly by $\bar{n}_i = \sum_j n_j w(i-j, \bar{n}_i)$. In turn, the weight function $w(i-j, \rho)$ is such that both the density and the DCF of the fluid are recovered in the homogeneous limit. In the Tarazona WDA, the further assumption is made that the weight function is a second-order polynomial in the density ρ. We thus have a well-defined algorithm for building up the excess free energy and, eventually, the density functional that is used to trace the conditions for fluid–solid coexistence.

Once the free energy of the reference system is given, we are left with the problem of incorporating the attraction Δv into the density functional of the t system using equation (16). We shall distinguish between the fluid and the solid, although this way the HKM functional

will only approximately be the same for all phases (this will have some harmful consequences for the interface structure; see section 5). While we obviously use for the fluid the reduced PDF of the homogeneous t system, as far as the solid is concerned we shall make the (apparently bad) approximation $g_{0,ij}[n] = 1$ outside the core, which is the same assumption as the mean-field approximation (MFA). In fact, we agree with Mederos *et al* [10] that the PDF of the low-temperature solid is *trivial*, since all the structure (which in a fluid is accounted for by the reduced PDF) is already present at the level of n_i itself[3]. This is rather obvious at $T = 0$, where $g_{ij} = 1$ at the typical distances of the perfect solid, while being undefined elsewhere. For small, but non-zero temperatures, a quasi-random (ideal-gas-like) distribution of interstitials and vacancies would extend the result $g_{ij} \simeq 1$ to all distances outside the core region.

A more refined approximation for the attractive interaction would be that of [10]. This theory uses the same prescription for the solid and the fluid, based on the use of the compressibility sum rule. However, the implementation of this method is also very difficult and much more involved than ours. In particular, the two algorithms for minimization that are described in appendix B do both require the numerical evaluation of the density derivatives of the DFT functional, which is indeed a very difficult task to accomplish if the recipe of [10] is followed. For the sake of completeness, we have also attempted to use the method of [8]. This relies on two approximations: (i) the use of equation (16) for the t345 *fluid*; and (ii) the decomposition of the DCF of the inhomogeneous t345 system as the sum of the analogous function for the t system and a remainder $\Delta c_2(i - j, \rho)$, assumed to be zero inside the core and MSA-like outside this region. In fact, we found no stable liquid phase by this method.

Going back to our theory, we write the difference in grand potential between the triangular solid (whose density field can be parametrized by means of two numbers only; see below) and the fluid with equal T and μ as the minimum of

$$\begin{aligned}\Delta\Omega(n_A, n_B) = \Delta\Omega^{(t)}(n_A, n_B) + \frac{N}{4}k_BT\Bigg\{&3\beta v_3 n_A^2 + (12\beta v_4 + 6\beta v_5)n_A n_B \\ &+ (9\beta v_3 + 12\beta v_4 + 6\beta v_5)n_B^2 - 2\rho^2\sum_{n=3}^{5} z_n\beta v_n g_0(n, \rho) \\ &- \left(\rho\sum_{n=3}^{5} z_n\beta v_n g_0(n, \rho) + \frac{\rho^2}{2}\sum_{n=3}^{5} z_n\beta v_n\frac{\mathrm{d}g_0(n, \rho)}{\mathrm{d}\rho}\right)(n_A + 3n_B - 4\rho)\Bigg\}. \quad (21)\end{aligned}$$

Note that, in the above equation:

(i) n_A and n_B are the number densities in the sublattices A and B of occupied and unoccupied sites, respectively (see appendix B);

(ii) $\Delta\Omega^{(t)}$ is the functional for the t model, defined at equation (C.1);

(iii) z_n is the coordination number for the nth shell, that is $z_3 = 6$, $z_4 = 12$, and $z_5 = 6$; and

(iv) $g_0(n, \rho)$ is the value taken by the reduced PDF of the t fluid at the nth-neighbour separation.

Apart from a different density dependence in $\Delta\Omega$, the machinery needed for calculating the weighted densities $\bar{n}_A$ and $\bar{n}_B$ (and their derivatives) from the densities n_A and n_B remains the same as for the t model, illustrated in appendix C.

[3] It is clear that what we are referring to here as a 'solid' is just one of the four symmetry-related ergodic components which characterize the very dense system, i.e., the broken-symmetry phase which is singled out after choosing a condensation seed. Otherwise, the solid phase itself would be homogeneous.

The equations for n_A and n_B are then (see, for comparison, equations (C.2))

$$n_A^{-1} = 1 + \frac{1-\rho}{\rho}\exp\Bigg\{c_1(\rho) + \beta f^{exc}(\bar{n}_A) + n_A\beta f^{exc\prime}(\bar{n}_A)\frac{\partial \bar{n}_A}{\partial n_A} + 3n_B\beta f^{exc\prime}(\bar{n}_B)\frac{\partial \bar{n}_B}{\partial n_A} - \left[\rho\sum_n z_n\beta v_n g_0(n,\rho) + \frac{\rho^2}{2}\sum_n z_n\beta v_n\frac{\mathrm{d}g_0(n,\rho)}{\mathrm{d}\rho}\right] + 6\beta v_3 n_A + (12\beta v_4 + 6\beta v_5)n_B\Bigg\};$$

$$n_B^{-1} = 1 + \frac{1-\rho}{\rho}\exp\Bigg\{c_1(\rho) + \beta f^{exc}(\bar{n}_B) + \frac{1}{3}n_A\beta f^{exc\prime}(\bar{n}_A)\frac{\partial \bar{n}_A}{\partial n_B} + n_B\beta f^{exc\prime}(\bar{n}_B)\frac{\partial \bar{n}_B}{\partial n_B} - \left[\rho\sum_n z_n\beta v_n g_0(n,\rho) + \frac{\rho^2}{2}\sum_n z_n\beta v_n\frac{\mathrm{d}g_0(n,\rho)}{\mathrm{d}\rho}\right] + (4\beta v_4 + 2\beta v_5)n_A + (6\beta v_3 + 8\beta v_4 + 4\beta v_5)n_B\Bigg\}. \tag{22}$$

In appendix B, we have outlined two different numerical algorithms for solving the minimum problem for a functional of the kind of (21).

We conclude our survey of the method with a few words about the liquid–vapour phase transition in the t345 model. The generalized grand potential of the homogeneous t345 system is $\Omega_\mu(\rho) = F(\rho) - N\mu\rho \equiv N(a(\rho) - \mu\rho)$, where

$$\beta a(\rho) = \rho\ln\rho + (1-\rho)\ln(1-\rho) + \rho\beta f^{exc}(\rho) + \tfrac{1}{2}\rho^2\sum_{n=3}^{5} z_n\beta v_n g_0(n,\rho). \tag{23}$$

At low enough temperature, there exists an interval of μ-values where there are two distinct minima of $\Omega_\mu(\rho)$, corresponding to the competing vapour and liquid phases (while the deeper minimum yields the physical solution, the other is associated with a metastable state). In particular, if we call ρ_v and ρ_l the related densities, the coexistence of the two phases occurs when the minima are equal:

$$\Omega_\mu(T,\rho_v) = \Omega_\mu(T,\rho_l) \qquad \text{and} \qquad \Omega'_\mu(T,\rho_v) = \Omega'_\mu(T,\rho_l) = 0. \tag{24}$$

The above equations are easily identified with the thermodynamic conditions for phase coexistence, i.e., equal values of T, P (the pressure), and μ for the two phases. This will automatically give rise to the Maxwell construction for the pressure and will also provide the right position for cutting the non-monotonic profile $a'(\rho)$ of the chemical potential as a function of the density.

4. DFT results: bulk

In this section, we present the results that we have obtained for the bulk properties of the t345 model by the lattice-DFT method outlined in the previous section. In order to check them, we have resorted to the MC simulation. In a typical grand-canonical MC experiment, a lattice-gas system is driven to equilibrium by a series of moves (creation or annihilation of one particle at a time), which are designed in such a way as to satisfy detailed balance (for more details, the reader is referred to [13]). In particular, a first-order transition is located at those values of T and μ where the number-density histogram of a large system sample shows two peaks of equal height, signalling that two distinct phases are equally stable.

We first review our results for the t model. We have formulated two different DFTs for the freezing of this model, i.e., the RY theory and the WDA of Tarazona. While the results of the former are discussed in appendix B, an outline of the latter can be found in appendix C.

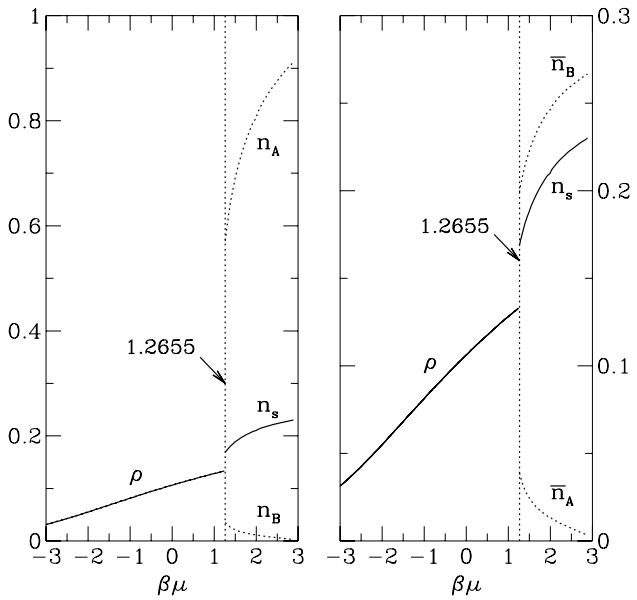

Figure 1. The t model (MSA + WDA). Left panel: total density (ρ in the fluid phase, n_s in the solid phase) versus reduced chemical potential. The sublattice densities, n_A and n_B (dotted lines), are also plotted in the solid region. Right panel, solid region: the weighted densities, $\bar{n}_A$ and $\bar{n}_B$, versus reduced chemical potential (we have used E1 for extending the definition of $f^{exc}(\rho)$ beyond $\rho = 0.21$).

Both theories rely on a MSA description for the fluid. Within the WDA theory, the densities of the coexisting fluid and solid are found to be $\rho_f = 0.1335$ and $\rho_s = 0.1686$—whence, a considerably larger density jump is predicted at the transition than given by the RY theory. Anyway, these numbers are still very far from those obtained by MC, i.e., $\rho_f = 0.172(1)$ and $\rho_s = 0.188(1)$, indicating that the instability of the t fluid against the solid is strongly anticipated in the WDA. As for the chemical-potential value at coexistence, the agreement with MC is also poor: while the WDA gives (through equations (A.4) and (A.5)) $\mu_c = 1.2655V$, MC yields instead $\mu_c = 1.725(5)V$.

In figure 1, the local and the weighted density of the t model are separately plotted for the two sublattices as a function of the chemical potential. In particular, the weighted density takes its larger value in the interstitial region, that is in the B sublattice. This is a counterintuitive effect which, however, is not peculiar to the lattice, being also found in the continuum (see, for instance, [4]).

Moving to the t345 model, we first checked the existence of two distinct fluid phases at low temperature. The liquid–vapour coexistence line is drawn by solving equations (23) and (24) (see figure 2). This gives a critical point at $t_{cr} = 1.27(1)$ and $\rho_{cr} = 0.079(2)$ (hereafter, reduced units $t = kT/V$ are used for the temperature). Also shown in figure 2 is the coexistence line as predicted by the MFA. The latter also uses equation (23), but with a 1 in place of $g_0(n, \rho)$.

Finally, we have minimized the density functional (21) in order to obtain the freezing and melting lines of the t345 model. It is right at this point that the choice between E1 and E2 (for extrapolating $f^{exc}(\rho)$ beyond $\rho = 0.21$, see appendix B) becomes crucial. In fact, while the solid phase never becomes stable—below a certain temperature—if E1 is adopted, we never run into trouble if extrapolation E2 is used. Anyway, E2 gives practically the same results as E1 at high temperature.

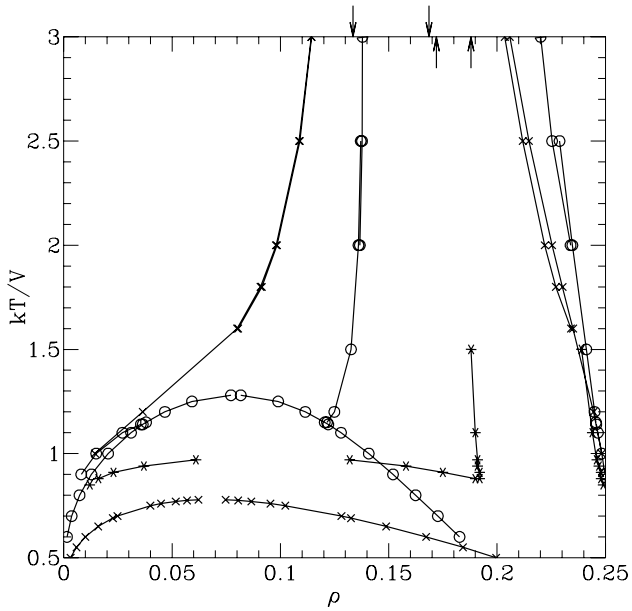

Figure 2. The phase diagram of the t345 model, using the t model (MSA + WDA) as a reference. Two distinct approximations for the perturbation part are compared through the respective phase diagrams: equation (21) (○) versus the MFA (×). The freezing and melting lines are constructed through the use of E1 at high T and of E2 at low T. For comparison, we show as asterisks some MC data points for a 48×48 lattice (MC averages are taken over 5×10^5 equilibrium sweeps; the errors affecting these points are of the same size as the symbols). The lines connecting the points are just a guide for the eye. The arrows pointing downwards mark the densities of the coexisting fluid and solid in the t model, as drawn from MSA + WDA. The other arrows mark the MC values for the same quantities.

The complete DFT phase diagram of the t345 model is plotted in figure 2 (open circles), together with the results of the MFA (crosses) and MC simulation (asterisks). To our delight, a triple point eventually shows up in the t345 phase diagram, at $t_{tr} = 1.145(5)$ and $\rho_{tr} = 0.122(1)$, as long as different forms of the perturbation part are used in the HKM functional for the solid and for the fluid. In other words, the use of g_0 for the description of the reduced PDF of the fluid turns out to be essential for obtaining a liquid region in the phase diagram. The liquid phase is unstable if the MFA is used also for the fluid. However, the agreement of our DFT with the MC results is mainly qualitative: the exact coordinates of the triple point are very different, $t_{tr}^{MC} = 0.87(1)$ and $\rho_{tr}^{MC} = 0.191(1)$; only the ratio of t_{tr} to t_{cr} is similar.

As an example, we have plotted in figure 3 the μ-evolution of the DFT number density at $t = 1.2$, upon going across the two phase transitions. Finally, figure 4 shows the DFT phase diagram of the t345 model in the T–μ plane, where we recognize the typical fork with two teeth of different length. In the same picture, the MC data points of figure 2 are also reported for comparison.

We have studied the t3 model with the same DFT as described above in order to check the internal consistency of our method. For this model, equation (23) with $v_4 = v_5 = 0$ never produces two distinct fluid phases, and the freezing and melting lines are similar to those found by the simpler RY theory (see figure 5). This result can be rationalized as follows: in the t345 model, the existence of attractive sites at the 'interstitial' distances r_4 and r_5 causes the upper stability threshold of the fluid phase to move up in density with respect to the t3 model,

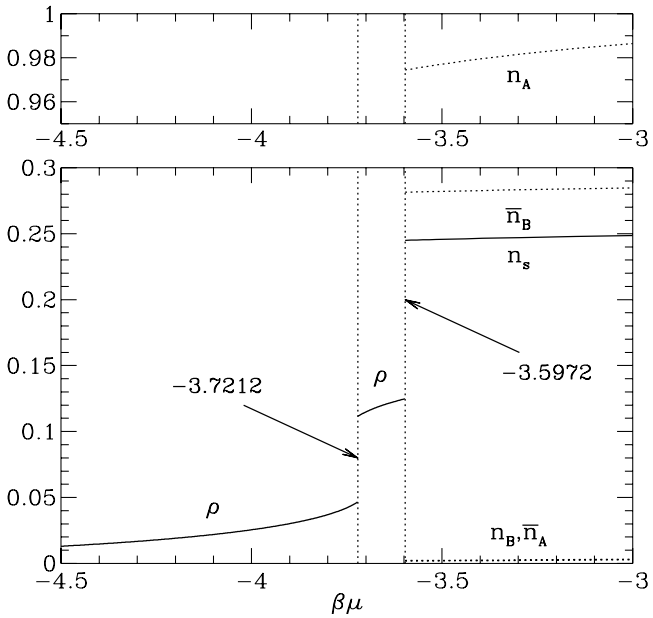

Figure 3. The t345 model (MSA + WDA + perturbation). The picture shows the $\beta\mu$-evolution of the overall density—ρ for the fluid and $n_s = (n_A + 3n_B)/4$ for the solid—along the isotherm $t = 1.2$. In the solid region, the real and weighted densities are separately plotted for the two sublattices A and B as dotted lines (note that n_B and $\bar{n}_A$ are almost indistinguishable). The dotted vertical lines mark the points where the phase transitions occur.

thus contributing to unveiling the triple point. This effect is missing in the t3 model, which thus fails to become a liquid. The conclusion, in perfect agreement with MC, is that no liquid phase is present in the t3 model.

Finally, we make a comment on the possible causes of the quantitative failure of our DFT for the t345 model. On one hand, one generally expects mean-field theory to work well in 3D, less so in 2D. One should also not forget that the perturbation formula (16) is a high-temperature approximation and that, at variance with the continuum case, there is no Barker–Henderson criterion which can be called upon for optimizing the hard-core diameter of the reference system. On the other hand, the low quality of the MSA for the reference t fluid is also partly responsible for the wrong position of the freezing and melting lines. To overcome this problem, we have made an attempt to replace the MSA with the hypernetted-chain approximation (HNCA) as a closure for the OZ relation of the homogeneous t system. For this model, the HNCA assumes: (i) $h(0) = h(1) = h(2) = -1$ (here, the argument is the shell number); (ii) $C(i-j,\rho) = h(i-j,\rho) - \ln[1+h(i-j,\rho)]$, outside the core. In practice, we should also assume that C and h are exactly zero beyond a certain distance, and we have chosen this to be the distance of the 38th neighbours (i.e., $6\sqrt{3}$). The solution method is iterative: at a given ρ, we make an initial estimate of $C(0), C(1), C(2)$ and $h(3), h(4), \ldots$, which are then updated using the inverse of the Fourier transform (15). Unfortunately, however, this works only up to $\rho = 0.11$, which is too small a density for allowing us to build an accurate reference-fluid free energy. Just in order to appreciate the difference between the two OZ closures, we have plotted in figure 6 the profiles, for $\rho = 0.1$, of the reduced PDF of the t model as given by the MSA and by the HNCA, respectively. The comparison with the 'exact' MC profile at the same density reveals the superiority of the MSA over the HNCA, which overestimates the

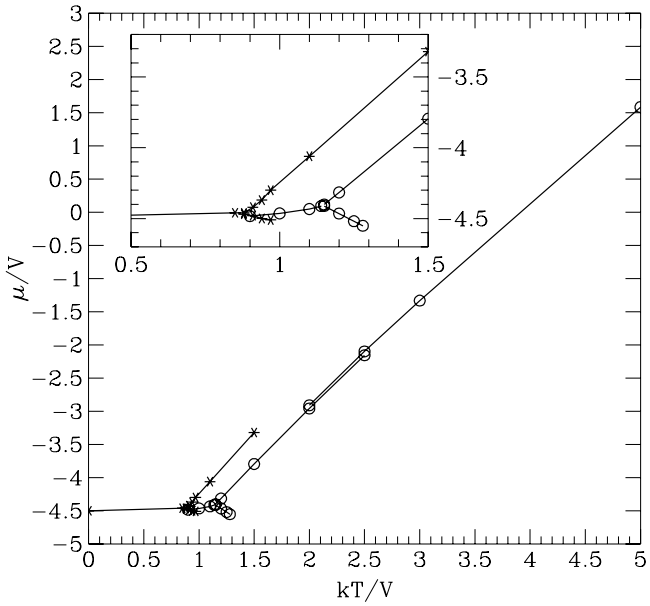

Figure 4. The t345 model (MSA + WDA + perturbation). The DFT phase diagram of the t345 model (○) as it appears on the T–μ plane. The solid–fluid coexistence line is of the E1 type at high T, and of the E2 type at lower T-values. For comparison, we have also reported as asterisks the MC data for a 48×48 lattice. Straight lines are drawn through the symbols as a guide for the eye. The inset shows a zoom on the triple-point region.

structure of the PDF. However, a good fluid structure is not necessarily accompanied by good thermodynamic properties, and this is actually the case for the MSA of the t model.

5. DFT results: interfaces

Now that we have an accurate density functional for the bulk of the t345 system, we move on to consider the structure of the interface between two coexisting bulk phases. Many similar calculations have been carried out in the past (see, for instance, [11, 15, 20]) and, in fact, the development of more and more careful DFT-based microscopic descriptions of the density profile across an interface has been historically a recurrent *leitmotif* [2].

Here, two cases are analysed which will deserve a rather different treatment: the liquid–vapour interface, i.e., the interface between two homogeneous phases, and the solid–fluid interface, which instead separates a broken-symmetry phase from a homogeneous one.

5.1. Liquid–vapour coexistence

As a first example, we have studied the interface between the coexisting liquid and vapour phases of the t345 model. This interface is assumed to lie perpendicularly to the y-direction. Horizontal layers are labelled with an integer λ, which is taken to be zero at the 'centre' of the interface. Since both phases are homogeneous, the density will be uniform along the x-direction, its value being a constant, ρ_λ, for all sites i of the λth layer. Let ρ_l and ρ_v be the densities of the coexisting phases at a given temperature T. Then, the common value μ of the chemical potential is $a'(\rho_v) = a'(\rho_l)$ (with $a(\rho)$ defined at equation (23)). For these T and μ, the grand potential per site of the bulk vapour or liquid is $a(\rho_v) - \mu\rho_v = a(\rho_l) - \mu\rho_l$. Given

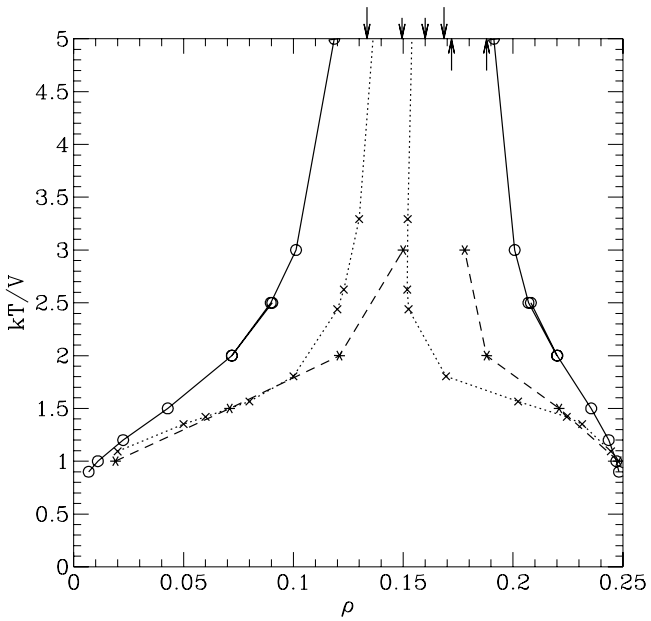

Figure 5. The phase diagram of the t3 model. Two distinct DFTs are contrasted through the respective t3 phase diagrams: one theory uses the t model (MSA + WDA) as a reference and the attractive interaction as a perturbation (O; the freezing and melting lines are constructed through the use of E1 at high T and of E2 at low T); the other theory is MSA + RY (×). MC data for a 48×48 lattice and 2×10^5 equilibrium sweeps are shown as asterisks. The straight lines between the points are plotted as a guide for the eye. The densities of the coexisting fluid and solid in the t model are marked as downward-pointing arrows (long and short arrows are for the MSA + WDA and the RY theory, respectively). The other arrows mark the MC estimates.

that, the generalized grand potential of the inhomogeneous system is

$$\beta\Omega_\mu[\rho] = N_x \sum_\lambda [\rho_\lambda \ln \rho_\lambda + (1-\rho_\lambda)\ln(1-\rho_\lambda) + \rho_\lambda \beta f^{exc}(\rho_\lambda)] + \frac{1}{2} N_x \sum_\lambda \rho_\lambda \sum_{j|i\in\lambda} n_j \beta\, \Delta v(|i-j|)\, g_0\left(i-j, \frac{\rho_\lambda + n_j}{2}\right) - N_x \beta\mu \sum_\lambda \rho_\lambda, \quad (25)$$

a functional of $\{\rho_\lambda\}$ subject to the conditions $\rho_\lambda \to \rho_l$ for $\lambda \to -\infty$ and $\rho_\lambda \to \rho_v$ for $\lambda \to +\infty$. As is usual practice [1], the g_0-function of the inhomogeneous t system at the $i-j$ lattice separation is represented by the fluid PDF as calculated for a density which is the arithmetic mean of the local densities in i and j. Finally, the grand-potential excess per surface particle due to the interface can be estimated as $\sigma(T) = \min_n \Sigma[n]$, where

$$\Sigma[n] = \frac{2\beta}{N_x}\{\Omega_\mu[n] - \Omega_\mu(\rho_v)\}. \quad (26)$$

The calculation of σ, which is nothing but the surface tension of the interface under consideration, proceeds in two steps: one first optimizes a simple exponential *ansatz* [15] and then refines the calculation via an unconstrained minimization that is accomplished in a way analogous to that followed for the bulk.

We have chosen, for a demonstration, a temperature of $t = 1.15$, which is slightly above the triple-point temperature. For this case, the shape of the liquid–vapour interface is plotted in figure 7. In this picture, the dotted curve represents the best exponential profile, while the continuous line is our final optimization. The surface tension is thus found to be $\sigma = 0.0145$.

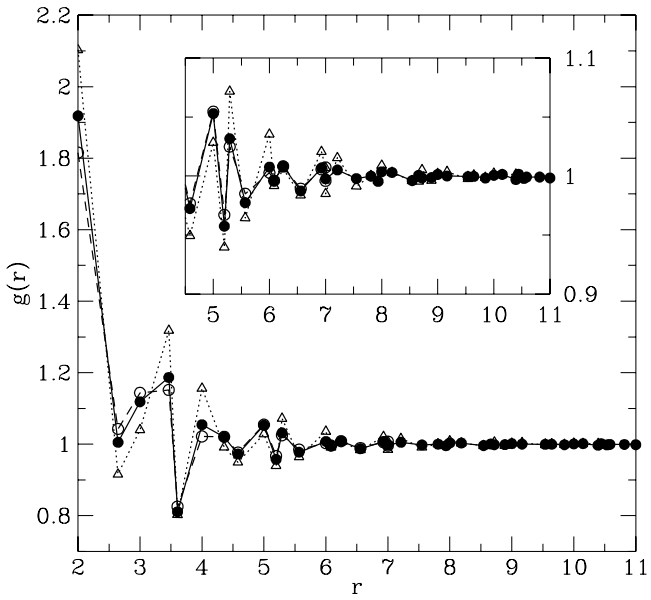

Figure 6. The homogeneous t model. Two distinct closures of the OZ relation are compared through the profile of the reduced PDF at $\rho = 0.1$: MSA (○ and dashed curve) and HNCA (△ and dotted curve). At the distances $r_{20} = 7$ of the 20th neighbours and $r_{33} = \sqrt{91}$ of the 33th neighbours, two symbols are reported for each curve (see the discussion following equation (C.4)). The full dots are the MC data points for a 48×48 sample at $\beta\mu = -0.32$ (here, the average density is $\langle c_i \rangle = 0.099\,95(1)$ over 5×10^5 equilibrium sweeps). Inset: a magnification of the large-distance region. It is clearly apparent that the MSA PDF is of overall better quality than the HNCA one.

By looking at figure 7, it appears that the deviation of the density profile from the exponential law is actually minute.

5.2. Solid–vapour coexistence

We have first analysed the structure of the solid–fluid interface in the t3 lattice gas by the RY theory, as built over the MSA DCF. To be specific, we consider a linear interface running along x. Such an interface breaks the translational symmetry along y, thus causing the sublattice densities to vary with y. Only very far from the interface do the densities recover the bulk values, being those of the solid, say, far below the interface and those of the coexisting fluid far above. The horizontal layers are labelled with an integer index, λ, which increases upon moving from the solid to the fluid region, being zero at the interface. We choose e.g. odd λ-values for those layers where particles are hosted in the $T = 0$ solid. At variance with the bulk case, we must distinguish *three* sublattices since we generally expect different density values at the interstitial sites pertaining to the even and to the odd layers. We call the sublattice formed by the interstitial sites in the odd layers C, and the other B. Finally, A is the triangular sublattice which is occupied in the $T = 0$ solid. We note that a C site has two adjacent A sites on the same layer. Conversely, the two closest A sites of a B site stay on the (odd) layers which are respectively below and above the (even) layer which the B site belongs to.

In the RY theory, the sublattice densities are drawn from equation (11) with $\mu_i = \mu$ (given by equation (A.5)) and a linear density functionality is assumed for the one-point DCF:

$$c_i^{(1)}[n] = c_1(\rho) + \sum_j c_2(i - j, \rho)(n_j - \rho), \tag{27}$$

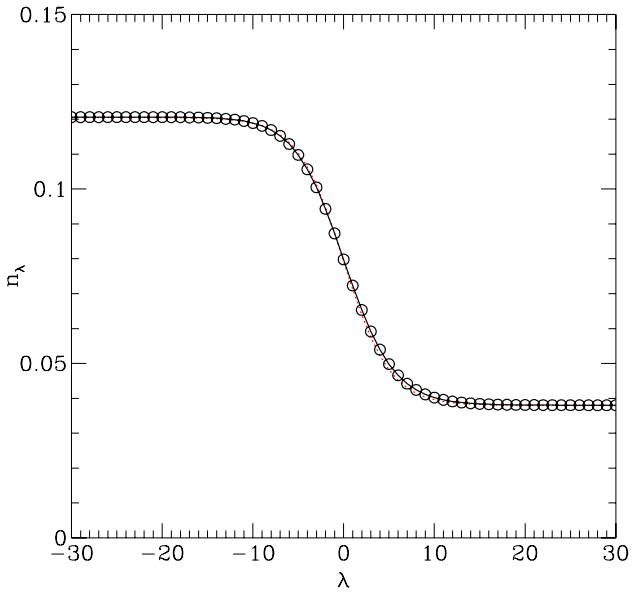

Figure 7. The t345 model (MSA + WDA + perturbation). The figure shows the density profile across the interface between the coexisting liquid and vapour phases at $t = 1.15$. The starting point of the functional minimization is an exponential profile (dotted curve); the open dots (which, for clarity, are joined by a continuous curve) are the final outcome of the optimization. It turns out that the difference between the two curves is very small.

where i can belong to A, B, or C. In particular, for the odd values of λ we have

$$\begin{aligned}
c^{(1)}(A,\lambda) &= c_1(\rho) + c_2(0,\rho)(n_{A,\lambda} - \rho) + 2c_2(1,\rho)(n_{B,\lambda-1} + n_{C,\lambda} + n_{B,\lambda+1} - 3\rho) \\
&\quad + c_2(2,\rho)(n_{C,\lambda-2} + 2n_{B,\lambda-1} + 2n_{B,\lambda+1} + n_{C,\lambda+2} - 6\rho) \\
&\quad + 2c_2(3,\rho)(n_{A,\lambda-2} + n_{A,\lambda} + n_{A,\lambda+2} - 3\rho); \\
c^{(1)}(C,\lambda) &= c_1(\rho) + c_2(0,\rho)(n_{C,\lambda} - \rho) + 2c_2(1,\rho)(n_{B,\lambda-1} + n_{A,\lambda} + n_{B,\lambda+1} - 3\rho) \\
&\quad + c_2(2,\rho)(n_{A,\lambda-2} + 2n_{B,\lambda-1} + 2n_{B,\lambda+1} + n_{A,\lambda+2} - 6\rho) \\
&\quad + 2c_2(3,\rho)(n_{C,\lambda-2} + n_{C,\lambda} + n_{C,\lambda+2} - 3\rho),
\end{aligned} \tag{28}$$

while, for the even values of λ,

$$\begin{aligned}
c^{(1)}(B,\lambda) &= c_1(\rho) + c_2(0,\rho)(n_{B,\lambda} - \rho) \\
&\quad + c_2(1,\rho)(n_{A,\lambda-1} + n_{C,\lambda-1} + 2n_{B,\lambda} + n_{A,\lambda+1} + n_{C,\lambda+1} - 6\rho) \\
&\quad + c_2(2,\rho)(n_{B,\lambda-2} + n_{A,\lambda-1} + n_{C,\lambda-1} + n_{A,\lambda+1} + n_{C,\lambda+1} + n_{B,\lambda+2} - 6\rho) \\
&\quad + 2c_2(3,\rho)(n_{B,\lambda-2} + n_{B,\lambda} + n_{B,\lambda+2} - 3\rho).
\end{aligned} \tag{29}$$

Next, the RY density functional is derived from equation (A.6), where it must be noted that

$$\begin{aligned}
\sum_{i,j} c_2(i-j,\rho)(n_i - \rho)(n_j - \rho) &= \sum_i (n_i - \rho)\{c_i^{(1)}[n] - c_1(\rho)\} \\
&= \frac{N_x}{2} \sum_{\lambda\ odd} (n_{A,\lambda} - \rho)\{c^{(1)}(A,\lambda) - c_1(\rho)\} \\
&\quad + N_x \sum_{\lambda\ even} (n_{B,\lambda} - \rho)\{c^{(1)}(B,\lambda) - c_1(\rho)\} \\
&\quad + \frac{N_x}{2} \sum_{\lambda\ odd} (n_{C,\lambda} - \rho)\{c^{(1)}(C,\lambda) - c_1(\rho)\}.
\end{aligned} \tag{30}$$

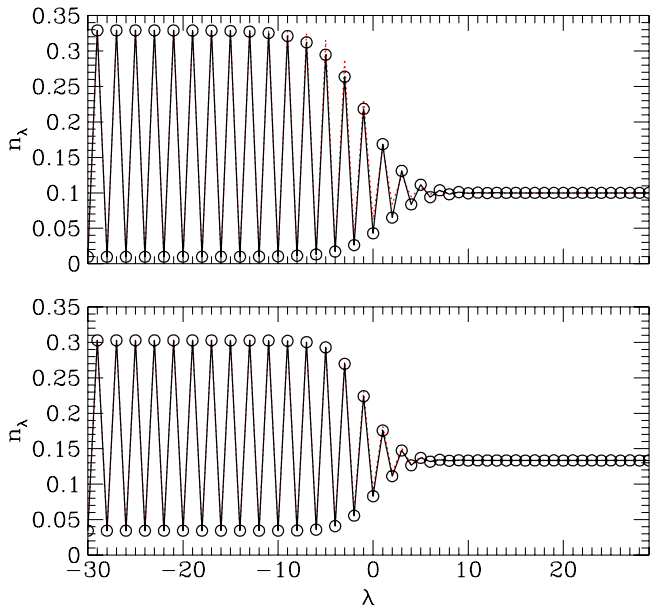

Figure 8. Top: the t3 model (MSA + RY), density profile across the solid–fluid interface at $t = 1.8036$ (here, $\rho_f = 0.1000$ and $\rho_s = 0.1695$). Bottom: the solid–fluid interface in the t model (MSA + WDA). In both panels, the optimal exponential profile (dotted curve) is contrasted with the outcome of an unconstrained $\Sigma[n]$ minimization (open dots and continuous curve).

As is clear, the final expression of the functional (A.6) is rather cumbersome and, therefore, we do not specify it here. Hence, we directly move to the numerical results.

We have considered just one temperature value, $t = 1.8036$. At this temperature, the fluid and solid coexistence densities are $\rho_f = 0.1000$ and $\rho_s = 0.1695$, respectively. Our slab consisted of 61 layers, from $\lambda = -30$ to 30 (at the boundaries, we have set the sublattice densities fixed to the solid values for $\lambda < -30$ and to the fluid value for $\lambda > 30$). To optimize the interface shape, we proceed in two steps: first, we attempt a rough optimization by the simple one-parameter *ansatz* [15]

$$\begin{aligned} n_{A,\lambda} &= \rho + \frac{n_A - \rho}{1 + \exp(\lambda/l)} \qquad (\lambda \text{ odd}); \\ n_{B,\lambda} &= \rho + \frac{n_B - \rho}{1 + \exp(\lambda/l)} \qquad (\lambda \text{ even}); \\ n_{C,\lambda} &= \rho + \frac{n_B - \rho}{1 + \exp(\lambda/l)} \qquad (\lambda \text{ odd}). \end{aligned} \tag{31}$$

The parameter l is chosen in such a way as to make (A.6) as low as possible. With that profile as a starting point, we run an iterative procedure, similar to that used for the bulk, for the unconstrained minimization of $\Omega_\mu[\rho] - \Omega_\mu(\rho_f)$. In the end, we get the density profile shown in figure 8 (top). At this temperature, the surface tension, given by equation (26), takes the value $\sigma = 0.0740(1)$.

Next, we move to the t model, as described by the WDA theory outlined in appendix C. From equation (A.5), we obtain the following expression for $\Sigma[n]$:

$$\Sigma[n] = \sum_{\lambda\ odd} \left[n_{A,\lambda} \ln \frac{n_{A,\lambda}}{\rho_v} + (1 - n_{A,\lambda}) \ln \frac{1 - n_{A,\lambda}}{1 - \rho_v} + n_{C,\lambda} \ln \frac{n_{C,\lambda}}{\rho_v} + (1 - n_{C,\lambda}) \ln \frac{1 - n_{C,\lambda}}{1 - \rho_v} \right]$$

$$+ 2 \sum_{\lambda\ even} \left[n_{B,\lambda} \ln \frac{n_{B,\lambda}}{\rho_v} + (1 - n_{B,\lambda}) \ln \frac{1 - n_{B,\lambda}}{1 - \rho_v} \right]$$
$$+ c_1(\rho_v) \sum_{\lambda\ odd} (n_{A,\lambda} + n_{C,\lambda} - 2\rho_v)$$
$$+ 2c_1(\rho_v) \sum_{\lambda\ even} (n_{B,\lambda} - \rho_v) + \sum_{\lambda\ odd} [n_{A,\lambda} \beta f^{exc}(\bar{n}_{A,\lambda})$$
$$+ n_{C,\lambda} \beta f^{exc}(\bar{n}_{C,\lambda}) - 2\rho_v \beta f^{exc}(\rho_v)]$$
$$+ 2 \sum_{\lambda\ even} [n_{B,\lambda} \beta f^{exc}(\bar{n}_{B,\lambda}) - \rho_v \beta f^{exc}(\rho_v)]. \tag{32}$$

For λ even, for example, the only weighted density that matters is $\bar{n}_{B,\lambda}$, which is defined in terms of all densities as

$$\bar{n}_{B,\lambda} = \sum_j n_j w(i - j, \bar{n}_{B,\lambda}), \tag{33}$$

where i is any particular site on the λth layer. For odd values of λ, one can analogously define $\bar{n}_{A,\lambda}$ and $\bar{n}_{C,\lambda}$. If we adopt the WDA method of Tarazona, then a result similar to equation (A.15) is obtained, giving $\bar{n}_{B,\lambda}$ in terms of the auxiliary quantities

$$\bar{n}_{kB,\lambda} = \sum_j n_j w_k(i - j) \qquad (\text{with } k = 0, 1, 2). \tag{34}$$

The explicit expression of (34) obviously requires the careful consideration of lattice sites j lying progressively further from the reference site i. As noted in appendix B, a sum such as (34) should in practice be truncated after a certain value of $|i - j|$, and we have chosen this to be the distance of the 20th neighbours. Even so, the final formula takes too many lines to be specified here, and is therefore omitted.

The actual minimization of $\Sigma[n]$ proceeds in a way analogous to the bulk case, described in appendix C. However, the formulae for the density derivatives of $\bar{n}_{A,\lambda}$, $\bar{n}_{B,\lambda}$, and $\bar{n}_{C,\lambda}$ are much more involved for the surface than for the bulk case. The outcome for the density profile across the interface is shown in figure 8 (bottom). Its shape is very similar to that of the t3 model, but the surface tension is much larger, our best result being $\sigma = 0.3182$.

We have finally considered the solid–vapour interface in the t345 model. In particular, we are interested in temperature values that are just below the triple-point temperature. In such conditions, and as long as surface melting occurs, a thin liquid-like film appears at the interface between the solid and the vapour. The functional $\Sigma[n]$ for the t345 system is the same as for the hard-core model plus the contribution coming from the attractive part of the potential:

$$\Sigma[n] = \Sigma^{(t)}[n] - \left(\rho_v \sum_n z_n \beta v_n g_0(n, \rho_v) + \frac{\rho_v^2}{2} \sum_n z_n \beta v_n \frac{\mathrm{d} g_0(n, \rho_v)}{\mathrm{d}\rho_v} \right)$$
$$\times \left[\sum_{\lambda\ odd} (n_{A,\lambda} + n_{C,\lambda} - 2\rho_v) + 2 \sum_{\lambda\ even} (n_{B,\lambda} - \rho_v) \right]$$
$$+ \tfrac{1}{2} \sum_{\lambda\ odd} \left[n_{A,\lambda} \sum_{j|i\in A,\lambda} n_j \beta\, \Delta v(|i - j|) + n_{C,\lambda} \right.$$
$$\left. \times \sum_{j|i\in C,\lambda} n_j \beta\, \Delta v(|i - j|) - 2\rho_v^2 \sum_n z_n \beta v_n g_0(n, \rho_v) \right]$$
$$+ \sum_{\lambda\ even} \left[n_{B,\lambda} \sum_{j|i\in B,\lambda} n_j \beta\, \Delta v(|i - j|) - \rho_v^2 \sum_n z_n \beta v_n g_0(n, \rho_v) \right]. \tag{35}$$

The minimization of (35) is carried out along the same lines as for the reference t model, the only difference being in the novel density functionality of Σ, not in the way the weighted density and its derivatives are calculated from the sublattice densities.

However, we expect a number of oddities to follow from (35) because of the different functional forms of the solid and fluid free energies. In particular, the minimization of (35) cannot produce a density profile which, on the $\lambda > 0$ side of the interface, smoothly drops into the vapour one. In fact, contrary to the situation for the cases examined before, $\Sigma[n]$ does not identically vanish when n_i takes the constant value ρ_v (even larger is the difference, at the triple point, between $\Omega_\mu^{(s)}(\rho_l)$ and $\Omega_\mu^{(f)}(\rho_v)$, meaning that the obvious prerequisite for observing a genuine surface melting is not met). This mismatch can be quantified in terms of the difference between ρ_v and the homogeneous solution ρ_∞ to $\Omega_\mu^{(s)}(\rho_\infty) = \Omega_\mu^{(f)}(\rho_v)$. At $t = 1.14$, i.e., just below the triple-point temperature, we find $\rho_v = 0.0356$ and $\rho_\infty = 0.0288$ (the difference being smaller at a lower T).

A way out of this *impasse* could be that of imposing ρ_∞ as boundary value for $\lambda \to +\infty$, while maintaining the form (35) for $\Sigma[n]$. Obviously, in order to enforce this condition, the initial *ansatz* must be accordingly modified into

$$\begin{aligned} n_{A,\lambda} &= \rho_\infty + \frac{n_A - \rho_\infty}{1 + \exp(\lambda/l)} \qquad (\lambda \text{ odd}); \\ n_{B,\lambda} &= \rho_\infty + \frac{n_B - \rho_\infty}{1 + \exp(\lambda/l)} \qquad (\lambda \text{ even}); \\ n_{C,\lambda} &= \rho_\infty + \frac{n_B - \rho_\infty}{1 + \exp(\lambda/l)} \qquad (\lambda \text{ odd}). \end{aligned} \tag{36}$$

We are perfectly conscious that the solution proposed here just represents a stratagem for making equation (35) suited to also describe the solid surface. A correct description would in fact need a single functional for all the phases.

For future reference, we plot in figure 9 (top) the MC outcome for the x-integrated densities of the t345 model in a 60×128 slab with periodic boundary conditions along x and fixed densities at the y-boundary. To be precise, the densities are kept fixed at the $T = 0$ solid and vapour values in the eight layers lying on the extreme left and right of the picture. The temperature is $t = 0.87$, i.e., slightly below the exact triple point, whereas the chemical potential has been adjusted in order to attain phase coexistence. The occurrence of surface melting in the t345 model is demonstrated by the structure of the interface in the central part of the picture, which is compatible with that of a 'modulated' liquid which strongly feels the underlying crystal ordering.

In figure 9 (bottom), we have plotted the density profile across the solid–vapour interface at $t = 1.14$, as calculated through the minimization of $\Sigma[n]$. From a look at this figure, we see that there are a few layers, interposed between the solid and the vapour, where the values of the sublattice densities are intermediate between those of the coexisting solid and vapour and close, on average, to that of the incoming liquid ($\simeq 0.121$, at $t = 1.15$). Interestingly, further evidence (see figure 10) supports the surface-melting interpretation, namely the existence of a maximum in $n_{B,\lambda}$ near $\lambda = 0$, and of another, less pronounced, in $n_{C,\lambda}$. These maxima are neither present in the initial profile (36) nor occur in the interface profiles of the t and t3 models. Anyway, the thickness of the molten layer appears to be strongly underestimated by our DFT as compared to MC. Moreover, the comparison with another DFT theory of surface melting [11] also actually leads us to qualify our results as rather poor.

We are aware that the use of *ad hoc* boundary conditions in our DFT treatment of the solid–vapour interface may cast some doubts on the general significance of the results plotted in figures 9 (bottom) and 10. Certainly, we are not allowed to draw any reasonable estimate

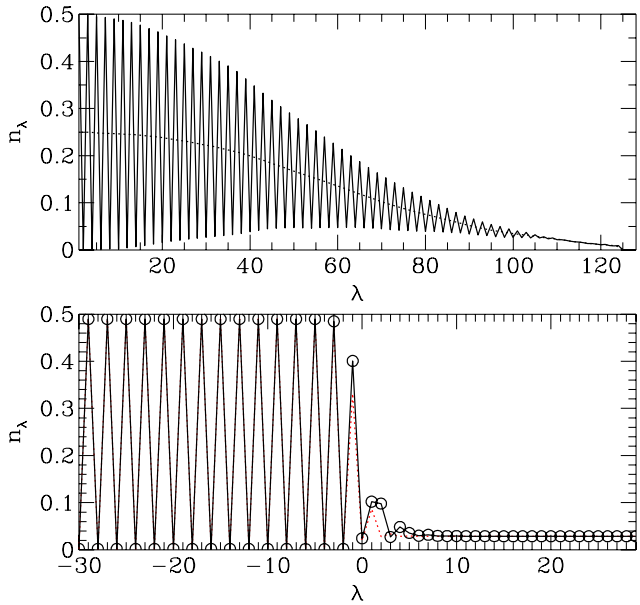

Figure 9. Top: the MC density profile across the solid–vapour interface of a t345 lattice system at $t = 0.87$, i.e., just below the triple-point temperature. To reach coexistence, the chemical potential is set equal to $\mu = -4.479V$. For a simulation box of 60×128, as many as 2×10^6 equilibrium sweeps were produced. The dotted line marks the average density over couples of adjacent layers. Near the centre of the picture, the maximum in the interstitial density (which is the bottom of the modulation) is the sign of a liquid-like behaviour. Bottom: DFT results for the t345 model (MSA + WDA + perturbation). The density profile across the solid–vapour interface is shown at $t = 1.14$: optimal exponential profile (dotted curve) versus unconstrained $\Sigma[n]$ minimization (open dots and continuous curve).

of the surface tension from the calculation that we have presented, which is quantitatively untenable. Notwithstanding the crudeness of our method, we nonetheless think that figures 9 (bottom) and 10 do genuinely capture the behaviour of the t345 system.

6. Conclusions

In this paper, we have used the lattice-DFT method to analyse the phase behaviour of a 2D lattice-gas model (named t345) which exhibits a solid, a liquid, and a vapour phase. Particles reside on a triangular lattice: occupation of nearest- and next-nearest-neighbour sites of a particle is forbidden, while the pair attraction extends from third to fifth neighbours.

We have built up an accurate solid structure for the purely hard-core model by working with the WDA of Tarazona, while the remaining part of the t345 potential has been treated as a mean field. This method is expected to provide good results both at very low and at very high temperatures, and to offer a not too bad interpolation in between.

In fact, our theory passes the crucial test of predicting the existence of a liquid phase in the t345 model. In particular, the ratio of the triple to the critical temperature is found to reproduce the exact value to within 2%. Another successful result is the prediction, in agreement with MC simulation, of the disappearance of the liquid phase when the range of the attraction is reduced to embrace third neighbours only. The main drawback of the theory is in the estimate of the freezing as well as of the melting density which, in the worst case, fall short of the

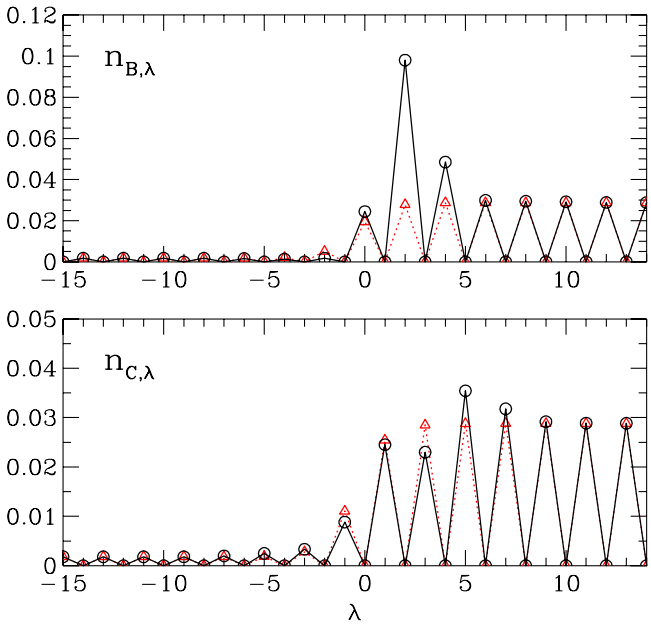

Figure 10. The t345 model (MSA + WDA + perturbation). The profile of $n_{B,\lambda}$ and $n_{C,\lambda}$ versus λ for the same solid–vapour interface as is represented in figure 9 (bottom). The unconstrained minimum-$\Sigma[n]$ profile (open dots and continuous curves) is compared with the best exponential *ansatz* (dotted curve). The maxima near $\lambda = 0$ are a sign of the local onset of a liquid-like behaviour.

(This figure is in colour only in the electronic version)

exact values by about 35%. This inconvenience should be ascribed to, besides the crudeness of the MFA approach (also worsened by the low system dimensionality), also the low quality of the MSA for the hard-core fluid (the HNCA is not viable since it does not converge even at moderate densities).

Having produced a qualitatively sound bulk theory, we have moved to a description of the interface structure in the t345 model. The same functional as was built up for the bulk system has been used to describe the coexistence between the solid and the vapour phases. Actually, the use of slightly different functional forms for the generalized grand potentials of the solid and of the vapour forces us to introduce a spurious boundary condition on the vapour side of the interface. If we allow for this artifice, we do in fact observe the appearance, just below the triple-point temperature, of a very thin liquid-like layer in between the solid and the vapour, which is the sign of the occurrence of surface melting in the system. However, it should be admitted that this slight evidence is not comparable, as for quality, to e.g. that provided by the 3D continuum DFT of [11].

Appendix A. The lattice DFT of freezing—generalities

In this appendix, we first derive a general expression for the generalized grand potential of an inhomogeneous lattice-gas system; this is then used for formulating a lattice DFT of freezing. In particular, we show how to adapt the WDA of Tarazona [3] to a lattice problem.

Let us suppose that we know the DCF $c_{ij}^{(2)}$ of a lattice system and the value of its $F^{exc}[n]$ for a given density profile n_0. Let $n_{\lambda i} = n_{0i} + \lambda\,\Delta n_i$, with $\Delta n_i = n_i - n_{0i}$ and $0 \leqslant \lambda \leqslant 1$. It

then follows from the first of equations (10) that

$$\beta F^{exc}[n] = \beta F^{exc}[n_0] - \sum_i \Delta n_i \int_0^1 \mathrm{d}\lambda\, c_i^{(1)}[n_\lambda]. \tag{A.1}$$

The functional $c^{(1)}$ can be similarly obtained, using the second of equations (10), as an integral of $c^{(2)}$, which eventually yields the exact formula:

$$\beta F^{exc}[n] = \beta F^{exc}[n_0] - \sum_i c_i^{(1)}[n_0]\,\Delta n_i - \sum_{i,j} \Delta n_i\,\Delta n_j \int_0^1 \mathrm{d}\lambda \int_0^\lambda \mathrm{d}\lambda'\, c_{ij}^{(2)}[n_{\lambda'}], \tag{A.2}$$

where the first two terms on the rhs of (A.2) identically vanish when choosing $n_0 = 0$. Actually, an infinite series of terms is hidden behind the last term of equation (A.2), each containing an order of the DCF as calculated for n_0. In practice, one could stop this infinite regression at the second order by approximating $c_{ij}^{(2)}[n_{\lambda'}]$ with $c_{ij}^{(2)}[n_0]$, and this gives the so-called RY theory [18].

Using equation (A.2), the excess free energy per particle of a fluid with density ρ can be generally written as

$$\beta f^{exc}(\rho) = -\frac{1}{\rho}\int_0^\rho \mathrm{d}\rho'\,(\rho - \rho')\tilde{c_2}(0, \rho'), \tag{A.3}$$

whereas $\rho f^{exc}(\rho)$ is the excess free energy *per site*. The function c_2 is calculated by augmenting the OZ relation with a closure, that is a further relation between the total and the DCF. We also quote the expression for c_1:

$$c_1(\rho) = -\beta f^{exc}(\rho) - \rho\beta f^{exc\prime}(\rho), \tag{A.4}$$

from which the chemical potential follows through equation (11):

$$\beta\mu = \ln\frac{\rho}{1-\rho} - c_1(\rho). \tag{A.5}$$

In order to study the coexistence between the solid and the fluid, we must require equal values of T and μ for the two phases. Given equation (A.5), the departure $\Delta\Omega[n] = \Omega_\mu[n] - \Omega_\mu(\rho)$ of the generalized grand potential of the solid from that of the fluid can be written as

$$\begin{aligned}\beta\,\Delta\Omega[n] = &\sum_i \left[n_i \ln\frac{n_i}{\rho} + (1-n_i)\ln\frac{1-n_i}{1-\rho}\right] \\ &+ c_1(\rho)\sum_i (n_i - \rho) + \beta F^{exc}[n] - N\rho\beta f^{exc}(\rho),\end{aligned} \tag{A.6}$$

N being the total number of lattice sites. Every different choice of $F^{exc}[n]$ defines a class of (approximate) DFTs. The simplest choice, yet rarely a quantitatively accurate one, is the RY theory, which leads to

$$\beta\,\Delta\Omega[n] = \sum_i \left[n_i \ln\frac{n_i}{\rho} + (1-n_i)\ln\frac{1-n_i}{1-\rho}\right] - \frac{1}{2}\sum_{i,j} c_2(i-j,\rho)(n_i-\rho)(n_j-\rho). \tag{A.7}$$

The RY theory already represents a considerable improvement over the ordinary MFA, which is tantamount to assuming $c_2(i-j,\rho) = 0$ for $i - j$ inside the core region, and $c_2(i-j,\rho) = -\beta v(|i-j|)$ outside the core. At variance with the MFA, the RY theory uses a DCF which is adjusted to fit the homogeneous OZ relation as supplemented with a proper closure. For instance, in the MSA, one requires that $g(i-j,\rho) = 0$ inside the core, while still assuming $c_2(i-j,\rho) = -\beta v(|i-j|)$ outside this region. A further possibility would be the PYA, which assumes $c_2(i,\rho) = g(i,\rho)[1 - \exp(\beta v(|i|))]$.

A more accurate, non-perturbative expression for $F^{exc}[n]$ is obtained by the so-called WDA [3, 4], which amounts to approximating the exact equation (A.2) for $n_0 = 0$ as

$$F^{exc}[n] \approx F^{exc}_{WDA}[n] \equiv \sum_i n_i f^{exc}(\bar{n}_i), \tag{A.8}$$

where the weighted density $\bar{n}_i$ is implicitly defined by

$$\bar{n}_i = \sum_j n_j w(i-j, \bar{n}_i). \tag{A.9}$$

The weighted density is required to be constant, i.e., $\bar{n}_i = \rho$, for a homogeneous system of density ρ (hence, $\tilde{w}(0, \rho) = \sum_j w(i-j, \rho) = 1$ for any i); moreover, the weight function w must be such that the DCF of the fluid be recovered in the homogeneous limit:

$$-\beta \frac{\partial^2 F^{exc}_{WDA}}{\partial n_i \, \partial n_j}\bigg|_{n_i=\rho} = c_2(i-j, \rho). \tag{A.10}$$

With the above requirements, the approximation obtained for $F^{exc}[n]$ is better than any truncated DCF expansion [4].

Using simple calculus, one can translate equation (A.10) into a differential equation for the Fourier transform of $w(i, \rho)$:

$$-\frac{1}{\beta}\tilde{c_2}(q, \rho) = 2f^{exc\prime}(\rho)\tilde{w}(q, \rho) + \rho f^{exc\prime\prime}(\rho)\tilde{w}^2(q, \rho) + 2\rho f^{exc\prime}(\rho)\tilde{w}(q, \rho)\tilde{w}'(q, \rho). \tag{A.11}$$

Although equation (A.11) can be numerically solved for any q and ρ [4], we here adopt the simpler recursive method of Tarazona [3], which considers a series expansion of $\tilde{w}(q, \rho)$ in powers of the density. If we stop at the second order, all we need to determine is

$$w(i, \rho) = w_0(i) + \rho w_1(i) + \rho^2 w_2(i) \tag{A.12}$$

from the knowledge of the lower-order terms in the two expansions

$$\begin{aligned} f^{exc}(\rho) &= f_1\rho + f_2\rho^2 + f_3\rho^3 + \cdots \\ c_2(i, \rho) &= \chi_0(i) + \rho\chi_1(i) + \rho^2\chi_2(i) + \cdots . \end{aligned} \tag{A.13}$$

We notice that equation (A.3) allows us to express f_{k+1} ($k = 0, 1, 2, \ldots$) in terms of χ_k as

$$\beta f_{k+1} = -\frac{1}{(k+1)(k+2)} \sum_i \chi_k(i). \tag{A.14}$$

Upon inserting equations (A.12) and (A.13) into (A.11) and equating term by term, we eventually obtain the general formulae:

$$\begin{aligned} w_0(i) &= -\frac{\chi_0(i)}{2\beta f_1}; \\ \tilde{w_1}(q) &= -\frac{\tilde{\chi_1}(q) + 4\beta f_2\tilde{w_0}(q) + 2\beta f_2\tilde{w_0}^2(q)}{2\beta f_1(1+\tilde{w_0}(q))}; \\ \tilde{w_2}(q) &= -\frac{\tilde{\chi_2}(q) + 6\beta f_3\tilde{w_0}(q) + 4\beta f_2\tilde{w_1}(q) + 6\beta f_3\tilde{w_0}^2(q) + 8\beta f_2\tilde{w_0}(q)\tilde{w_1}(q) + 2\beta f_1\tilde{w_1}^2(q)}{2\beta f_1(1+2\tilde{w_0}(q))}. \end{aligned} \tag{A.15}$$

Given the weight function, the weighted density is explicitly determined from equation (A.9) in terms of the n_i as

$$\bar{n}_i = \frac{2\bar{n}_{0i}}{1 - \bar{n}_{1i} + \sqrt{(1-\bar{n}_{1i})^2 - 4\bar{n}_{0i}\bar{n}_{2i}}}, \tag{A.16}$$

where $\bar{n}_{ki} = \sum_j n_j w_k(i-j)$ for $k = 0, 1, 2$. In practice, one uses equation (A.16) as part of the iterative procedure by which the DFT minimum principle is implemented numerically (see the details in appendix B). A practical demonstration of the WDA method will be given in appendix C.

Appendix B. RY theory for the t3 model

We hereby describe in detail how to work out a RY DFT for the t3 model. Our first task is to determine the DCF of the homogeneous system. We have chosen to solve numerically the OZ relation with the MSA closure. Let $a_x = \hat{x}$ and $a_y = (\sqrt{3}/2)\hat{y}$ be the primitive vectors of the triangular lattice (hereafter, we assume a unit lattice constant). Then, the reciprocal-lattice vectors are $b_x = 2\pi\hat{x}$ and $b_y = (4\pi\sqrt{3}/3)\hat{y}$. Any sum over Born–Von Karman vectors (see footnote 2) is written, in the infinite-size limit, as an integral over the first Brillouin zone:

$$\frac{1}{N}\sum_q f(q) \to \frac{\sqrt{3}}{2}\int_{BZ}\frac{\mathrm{d}^2q}{(2\pi)^2}\,f(q) = \frac{\sqrt{3}}{2}\int_{-\pi}^{\pi}\frac{\mathrm{d}q_x}{2\pi}\int_{-2\pi\sqrt{3}/3}^{2\pi\sqrt{3}/3}\frac{\mathrm{d}q_y}{2\pi}\,f(q_x,q_y)$$
$$= \int_{-\pi}^{\pi}\frac{\mathrm{d}q_x}{2\pi}\int_{-\pi}^{\pi}\frac{\mathrm{d}q'_y}{2\pi}\,f\left(q_x,\frac{2\sqrt{3}}{3}q'_y\right). \tag{B.1}$$

For the t3 fluid, the MSA assumes: (i) $C(3) = c_2(3) = -\beta v_3$ and $C(n) = 0$ for all $n > 3$ shells; (ii) $h(0) = h(1) = h(2) = -1$. From (ii), three equations are derived for the unknown quantities $C(0)$, $C(1)$, and $C(2)$. For instance, the first of these is obtained by plugging the OZ relation (15) into the expression $h(0) = (1/N)\sum_q \tilde{h}_q$. After a few manipulations, we eventually obtain the following set of equations:

$$2\rho(1-\rho)C(3) = \frac{z_3}{(2\pi)^2}\int_{-\pi}^{\pi}\mathrm{d}q_x\int_{-\pi}^{\pi}\mathrm{d}q_y\,\frac{1}{1-z_1f_1(q_x,q_y)-z_2f_2(q_x,q_y)-z_3f_3(q_x,q_y)};$$
$$-6\rho^2C(3) = \frac{z_3}{(2\pi)^2}\int_{-\pi}^{\pi}\mathrm{d}q_x\int_{-\pi}^{\pi}\mathrm{d}q_y\,\frac{f_1(q_x,q_y)}{1-z_1f_1(q_x,q_y)-z_2f_2(q_x,q_y)-z_3f_3(q_x,q_y)}; \tag{B.2}$$
$$-6\rho^2C(3) = \frac{z_3}{(2\pi)^2}\int_{-\pi}^{\pi}\mathrm{d}q_x\int_{-\pi}^{\pi}\mathrm{d}q_y\,\frac{f_2(q_x,q_y)}{1-z_1f_1(q_x,q_y)-z_2f_2(q_x,q_y)-z_3f_3(q_x,q_y)},$$

where $z_1 = 2\rho C(1)/(1-\rho C(0))$, $z_2 = 2\rho C(2)/(1-\rho C(0))$, and $z_3 = 2\rho C(3)/(1-\rho C(0))$ are auxiliary unknowns. Moreover,

$$\begin{aligned} f_1(q_x,q_y) &= \cos q_x + 2\cos(\tfrac{1}{2}q_x)\cos q_y;\\ f_2(q_x,q_y) &= \cos(2q_y) + 2\cos(\tfrac{3}{2}q_x)\cos q_y;\\ f_3(q_x,q_y) &= \cos(2q_x) + 2\cos q_x\cos(2q_y). \end{aligned} \tag{B.3}$$

For a given ρ, equations (B.2) are to be solved recursively: starting from estimates of z_1, z_2, and z_3, these quantities are gradually adjusted until the rhs of equations (B.2) becomes equal to the quantity on the respective lhs with a tolerance smaller than 10^{-8}.

Once the DCF has been determined, we can use e.g. the RY theory to construct the generalized grand potential of the t3 model. We call the triangular sublattice that is occupied in the $T = 0$ crystal A, while B includes the rest of the lattice. Then, the independent density variables are the two sublattice occupancies, n_A and n_B, while the solid density is $\rho_s = (n_A + 3n_B)/4$. The density functional that is to be minimized reads

$$\frac{4\beta\,\Delta\Omega(n_A,n_B)}{N} = n_A\ln\frac{n_A}{\rho} + (1-n_A)\ln\frac{1-n_A}{1-\rho} + 3\left[n_B\ln\frac{n_B}{\rho} + (1-n_B)\ln\frac{1-n_B}{1-\rho}\right]$$
$$-\tfrac{1}{2}[(c_2(0)+6c_2(3))(n_A-\rho)^2 + 12(c_2(1)+c_2(2))(n_A-\rho)(n_B-\rho)$$
$$+3(c_2(0)+4c_2(1)+4c_2(2)+6c_2(3))(n_B-\rho)^2], \tag{B.4}$$

where we have omitted to indicate the ρ-dependence of the c_2-values. If, after minimization, $\Delta\Omega$ happens to be negative, then the solid phase is stable; otherwise the fluid will overcome

the solid in stability. As a result, the locus of the $\Delta\Omega$ zeros allows us to draw the fluid–solid coexistence line in the T–ρ plane.

In order to find the minimum of $\Delta\Omega$, at least two different strategies can be pursued whose efficiencies turn out, in fact, to be comparable. The first method is to lay down, starting from somewhere in the $\{n_A, n_B\}$ space, a fictitious relaxational (steepest-descent) dynamics, i.e.,

$$n_A(t+\Delta t) = n_A(t) - \Delta t\,\frac{\partial\,\Delta\Omega}{\partial n_A}(t) \tag{B.5}$$

and similarly for n_B, where Δt is a conveniently small number. In the long run, the sublattice densities eventually stabilize, and this will signal that a minimum of $\Delta\Omega$ has been reached (note that there is always the possibility of getting stuck in a local minimum; so, one should check the nature of the minimum with different Δt values and initial conditions).

The other method is to solve, by a self-consistent procedure, the non-linear equations for the densities:

$$\begin{aligned} n_A^{-1} &= 1 + \frac{1-\rho}{\rho}\exp[-(c_2(0)+6c_2(3))(n_A-\rho) - 6(c_2(1)+c_2(2))(n_B-\rho)]; \\ n_B^{-1} &= 1 + \frac{1-\rho}{\rho}\exp[-2(c_2(1)+c_2(2))(n_A-\rho) \\ &\qquad - (c_2(0)+4c_2(1)+4c_2(2)+6c_2(3))(n_B-\rho)]. \end{aligned} \tag{B.6}$$

In order to reach a better convergence, we have resorted to a mixing scheme: at the kth step in the iteration, we use the inverse of the rhs of each equation (B.6) to obtain a trial estimate (denoted by a hat) of the densities at the $(k+1)$th step. Then, we assume $n_A^{(k+1)} = (1-q)n_A^{(k)} + q\hat{n}_A^{(k+1)}$ (and similarly for n_B), where q is a small positive number.

The RY freezing and melting lines of the t3 model are shown in figure 5 as dotted lines in the ρ–T plane. Since there is only one minimum in the fluid generalized grand potential, the t3 system shows, according this theory, two phases only—fluid and triangular solid, with a density gap becoming narrower and narrower with increasing temperature. In the same figure, we have marked with arrows the densities of the coexisting fluid and solid in the t model, namely $\rho_f = 0.1495$ and $\rho_s = 0.1600$ (see below). In fact, the t model can be viewed as the infinite-temperature limit of the t3 model.

The MSA equations for the t model can be easily adapted from those of the t3 model. An important thing to notice is that the iterative procedure by which the MSA is solved usually fails to converge beyond a certain density ρ_{up} which, for the t model, is slightly above 0.21. This is a well-known problem in the field of integral equations of classical fluids which, however, is not particularly dangerous in view of the fact that the fluid phase loses its stability against the solid well below ρ_{up}. This notwithstanding, we might have the need to extend, as required by the forthcoming WDA of appendix C, the definition of $f^{exc}(\rho)$ well beyond ρ_{up} (and even beyond 0.25). To this end, since the only obvious constraint to fulfil is regularity, the possible solutions are many. Following the proposal advanced in [21] for hard discs, we could assume, for instance, the (metastable-) fluid pressure to be exactly given, beyond $\rho = 0.21$, as

$$\frac{\beta P}{\rho} = \frac{1 + a'\eta + b'\eta^2 + c'\eta^3 + d'\eta^4}{(1-\eta)^2}, \tag{B.7}$$

where $\eta = (2\pi\sqrt{3}/3)\rho \equiv \alpha\rho$ is the packing fraction (corresponding to a hard-core diameter of 2), while a', b', c', and d' are free parameters. The excess free energy will follow from

$$\beta f^{exc}(\rho) = \int_0^\rho \left(\frac{\beta P(t)}{t} - 1\right)\frac{\mathrm{d}t}{t}, \tag{B.8}$$

which, through the density derivative of equation (A.5), is easily proved to be equivalent to equation (A.3). Upon inserting equation (B.7) into (B.8), we eventually arrive at the following analytic form:

$$\beta f^{exc}(\rho) = a\rho + b\rho^2 + \frac{c\rho}{1-\alpha\rho} + d\ln(1-\alpha\rho), \tag{B.9}$$

with other parameters a, b, c, and d. The latter are fixed by requiring a smooth behaviour at $\rho = 0.21$.

The problem with the above extrapolation (called E1) is that (B.9) blows up to infinity for $\rho = 1/\alpha \simeq 0.276$. This could be a serious inconvenience if one needs to calculate $f^{exc}(\rho)$ beyond $1/\alpha$. In this case, we resort to a simpler extrapolation (called E2), which merely expresses $f^{exc}(\rho)$ as a fourth-order polynomial beyond $\rho = 0.21$.

Appendix C. WDA for the t model

In the present appendix, we show how to build up a WDA theory for the t model.

Upon inserting (A.8) into (A.6), and specializing to the t model, we readily obtain

$$\begin{aligned}\frac{4\beta\,\Delta\Omega(n_A,n_B)}{N} &= n_A\ln\frac{n_A}{\rho} + (1-n_A)\ln\frac{1-n_A}{1-\rho} + 3\left[n_B\ln\frac{n_B}{\rho} + (1-n_B)\ln\frac{1-n_B}{1-\rho}\right] \\ &\quad + c_1(\rho)(n_A + 3n_B - 4\rho) + n_A\beta f^{exc}(\bar{n}_A) + 3n_B\beta f^{exc}(\bar{n}_B) - 4\rho\beta f^{exc}(\rho).\end{aligned} \tag{C.1}$$

If we impose the vanishing of the partial derivatives of (C.1), we get the equations for n_A and n_B:

$$\begin{aligned}n_A^{-1} &= 1 + \frac{1-\rho}{\rho}\exp\left[c_1(\rho) + \beta f^{exc}(\bar{n}_A) + n_A\beta f^{exc\prime}(\bar{n}_A)\frac{\partial\bar{n}_A}{\partial n_A} + 3n_B\beta f^{exc\prime}(\bar{n}_B)\frac{\partial\bar{n}_B}{\partial n_A}\right], \\ n_B^{-1} &= 1 + \frac{1-\rho}{\rho}\exp\left[c_1(\rho) + \beta f^{exc}(\bar{n}_B) + \frac{1}{3}n_A\beta f^{exc\prime}(\bar{n}_A)\frac{\partial\bar{n}_A}{\partial n_B} + n_B\beta f^{exc\prime}(\bar{n}_B)\frac{\partial\bar{n}_B}{\partial n_B}\right].\end{aligned} \tag{C.2}$$

In the above equations, the weighted densities $\bar{n}_A$ and $\bar{n}_B$ are calculated from equation (A.16). As for their density derivatives, it follows from the original definition (A.9) that

$$\frac{\partial\bar{n}_A}{\partial n_A} = (1 - \bar{n}_{1A} - 2\bar{n}_{2A}\bar{n}_A)^{-1}\left(\frac{\partial\bar{n}_{0A}}{\partial n_A} + \bar{n}_A\frac{\partial\bar{n}_{1A}}{\partial n_A} + \bar{n}_A^2\frac{\partial\bar{n}_{2A}}{\partial n_A}\right), \tag{C.3}$$

and similarly for other derivatives. In equation (C.3), $\bar{n}_{kA} = \sum_j n_j w_k(i-j)$, with $i \in A$ and $k = 0, 1, 2$. We thus have, for instance,

$$\begin{aligned}\frac{\partial\bar{n}_{kA}}{\partial n_A} &= \sum_{j\in A|i\in A} w_k(i-j) = w_k(0) + 6w_k(3) + 6w_k(6) + 6w_k(8) \\ &\quad + 12w_k(13) + 6w_k(15) + 6w_k(19) + \cdots,\end{aligned} \tag{C.4}$$

where we have used the shell number (rather than the distance) as the argument for w_k. Obviously, in order to make the whole procedure computationally feasible, the sum in equation (C.4) (and any other sum of the same kind) must be truncated at a certain distance, and we have chosen to stop summing beyond the distance (=7) of the 20th neighbours. This is not a problem, however, since the w_k-functions rapidly drop to zero when increasing the distance from the reference site.

We remark that a novel feature emerges in the behaviour of $w_k(i)$ right when we reach the distance of the 20th neighbours, which is not observed at the smaller distances. Two different groups of such neighbours are, in fact, to be distinguished: six of them are symmetry related,

as are the other twelve. But the value of w_k for a site of the first group is *different* from that calculated for a neighbour of the second group (hence we have a $w_k(20a)$ and a $w_k(20b)$). We should wait until the 33th-neighbour shell (at a distance of $\sqrt{91}$) to observe this feature repeated again. Hence, notwithstanding that the potential shows radial symmetry, w_k is *not* spherically symmetric and this is why, on a lattice, particular care must always be paid to distinguishing translational from spherical symmetry, although the exceptions to radial symmetry are, in a sense, rare [22]. Note that the reduced PDF behaves similarly to w_k, i.e., $g(i-j,\rho)$ is not spherically symmetric either.

References

[1] Evans R 1979 *Adv. Phys.* **28** 143

[2] Recent review articles on the DFT method, with special reference to the freezing of 3D continuous fluids, are
Baus M 1990 *J. Phys.: Condens. Matter* **2** 2111
Singh Y 1991 *Phys. Rep.* **207** 351
Evans R 1992 *Fundamentals of Inhomogeneous Fluids* ed D Henderson (New York: Dekker)
Löwen H 1994 *Phys. Rep.* **237** 249
Löwen H 2002 *J. Phys.: Condens. Matter* **14** 11897

[3] Tarazona P 1985 *Phys. Rev.* A **31** 2672

[4] Curtin W A and Ashcroft N W 1985 *Phys. Rev.* A **32** 2909

[5] The literature on the fundamental-measure theory is vast. We list just a number of significant contributions by its founder:
Rosenfeld Y 1989 *Phys. Rev. Lett.* **63** 980
Rosenfeld Y, Schmidt M, Löwen H and Tarazona P 1997 *Phys. Rev.* E **55** 4245
Rosenfeld Y 2002 *J. Phys.: Condens. Matter* **14** 9141

[6] Tarazona P and Rosenfeld Y 1997 *Phys. Rev.* E **55** R4873
Tarazona P 2000 *Phys. Rev. Lett.* **84** 694
Tarazona P 2002 *Physica* A **306** 243

[7] Schmidt M 1999 *Phys. Rev.* E **60** R6291
Schmidt M 2000 *J. Phys.: Condens. Matter* **11** 10163
and see also
Sweatman M B 2002 *J. Phys.: Condens. Matter* **14** 11921

[8] Curtin W A and Ashcroft N W 1986 *Phys. Rev. Lett.* **56** 2775

[9] Tang Z, Scriven L E and Davis H T 1991 *J. Chem. Phys.* **95** 2659

[10] Mederos L, Navascues G, Tarazona P and Chacon E 1993 *Phys. Rev.* E **47** 4284

[11] Ohnesorge R, Löwen H and Wagner H 1991 *Phys. Rev.* A **43** 2870
Ohnesorge R, Löwen H and Wagner H 1994 *Phys. Rev.* E **50** 4801

[12] Sweatman M B 2001 *Phys. Rev.* E **65** 011102

[13] Prestipino S 2000 *Phys. Rev.* E **62** 2177

[14] Nieswand M, Dieterich W and Majhofer A 1993 *Phys. Rev.* E **47** 718
Nieswand M, Majhofer A and Dieterich W 1994 *Phys. Rev.* E **48** 2521

[15] Reinel D, Dieterich W and Majhofer A 1994 *Phys. Rev.* E **50** 4744

[16] An G and Schick M 1989 *Phys. Rev.* B **39** 9722

[17] See for example
Hansen J-P and MacDonald I R 1986 *Theory of Simple Liquids* (New York: Academic)

[18] Ramakrishnan T V and Yussouff M 1979 *Phys. Rev.* B **19** 2775
Haymet A D and Oxtoby D W 1979 *J. Chem. Phys.* **74** 2559
Haymet A D and Oxtoby D W 1982 *J. Chem. Phys.* **76** 6262

[19] Lafuente L and Cuesta J A 2002 *J. Phys.: Condens. Matter* **14** 12079

[20] Curtin W A 1987 *Phys. Rev. Lett.* **59** 1228

[21] Baus M and Colot J L 1987 *Phys. Rev.* A **36** 3912

[22] Compare also
Prestipino S 2002 *Phys. Rev.* E **66** 021602